Applied Surface Science Advances 21 (2024) 100594

Contents lists available at ScienceDirect

Applied Surface Science Advances

journal homepage: www.sciencedirect.com/journal/applied-surface-science-advances

Deposition of thin films on basalt fibers surface by atmospheric pressure plasma with different siloxane precursors

Chengfeng Xiong [a,b,c], Ming Gao [a,*], Hao Huang [a], Yu Wang [a], Xiaobin Gu [a], Zilan Xiong [c], Yifan Huang [a]

[a] Shenzhen Institute of Advanced Technology, Chinese Academy of Sciences, Shenzhen 518055, China
[b] Nano Science and Technology Institute, University of Sciences and Technology of China, Suzhou 215123, China
[c] State Key Laboratory of Advanced Electromagnetic Technology, Huazhong University of Science and Technology, Wuhan, Hubei 430074, China

ARTICLE INFO

Keywords:
Thin films
Basalt fiber, plasma deposition
Siloxane precursors

ABSTRACT

In this study, surface modification of basalt fibers (BFs) utilizing atmospheric pressure plasma deposition was carried out. Using this one-step deposition approach, three siloxane precursors with different structures including methyltrimethoxysilane (MTMS), hexamethyldisiloxane (HMDSO), and tetramethoxysilane (TMOS) were deposited on BFs surface, respectively. The physicochemical properties of the thin films from three different siloxane compounds are elucidated. In comparison with MTMS-coated sample, HMDSO-coated and TMOS-coated BFs surfaces feature an improved thermal insulation performance. The results demonstrate that atmospheric pressure plasma deposition is an efficient approach to modify flexible materials surface with improved thermal insulation. Moreover, it provides a reference to decide which precursor type is preferred for certain applications.

1. Introduction

Basalt fibers (BFs) have attracted sustained attention due to their excellent chemical stability, good thermal resistance and low thermal conductivity [1,2]. Considering these merits, BFs have emerged as promising thermal insulation materials for various applications in military and civil engineering [3,4]. Nevertheless, the poor intrinsic surface properties of BFs due to the smooth surface and chemical inertness have been a challenge for high performance of BFs reinforced polymeric composites [5]. It is necessary to modify BFs surface in order to increase the interfacial strength of BFs reinforced composites. Plasma treatment has proved to be one of the most convenient and practical tactic for the surface modification of the fibers with the bulk properties maintained [6]. Such treatment method is beneficial for modifying the physical and chemical structures of the surface layer of the fibers. However, the plasma-treated surface easily loses the generated features as a result of aging with the time progresses [7].

In recent years, thin films deposition on BFs surface by plasma have been applied for improving the surface roughness of fibers and constructing a thin film structure. Using plasma deposition technology, thin film can be prepared on the fiber surface by a small amount of precursor in a solvent-free environment in one step [8]. Until now, there have been a few studies on the construction of micro-nano thin films on the BFs surface. Yu et al. modified BFs surface by plasma polymerization of 3-aminopropyltriethoxysilane (APTES), and the APTES can form a thick polymeric layer on the BFs surface [9]. Lilli et al. deposited a polymer film based on pure tetravinylsilane (TVS) or its mixture with two different oxygen amounts on BFs surface by plasma deposition [10]. Unfortunately, even though these depositions have shown promising results, their practical application is a challenging task for cost-effectiveness and complicated equipment reasons. Indeed, atmospheric pressure plasma deposition has been explored to be an alternative solution to low-pressure deposition process, due to its advantages of simple operation and low costs [11,12].

In atmospheric pressure plasma deposition process, the properties of the thin films are sensitive to the applied parameters, such as deposition time, deposition temperature, discharge power and so on [13–15]. More importantly, the type of the precursor is essential to control the basic components and modulate the physicochemical properties of the films. For example, Duran et al. unveiled the role of the structure and the chemistry of siloxane precursors in the anti-fogging performance of plasma-coated glass, and the results have shown that a cyclic siloxane structure is required to deposit an anti-fogging coating [16]. Egghe et al. compared the physicochemical properties and aging behavior of two

* Corresponding author.
E-mail address: ming.gao@siat.ac.cn (M. Gao).

https://doi.org/10.1016/j.apsadv.2024.100594
Received 26 September 2023; Received in revised form 12 January 2024; Accepted 14 March 2024
Available online 20 March 2024

different APTES-derived plasma polymer based coatings [17]. On this basis, the aim of this study is to modify BFs surface by atmospheric pressure plasma deposition, and three siloxane precursors with different structures including methyltrimethoxysilane (MTMS), hexamethyldisiloxane (HMDSO), and tetramethoxysilane (TMOS) are used to manipulate the physicochemical characteristics of the thin films. The property of plasma-deposited films is discussed in terms of surface morphology and surface chemistry, correlated with the structure of the siloxane precursors. The thermal stability of the thin films is measured by thermogravimetry analysis, and the thermal insulation performance of the thin films is assessed by measuring the surface temperature of the samples after being exposed to hot plate.

2. Materials and methods

2.1. Materials

Methyltrimethoxysilane (MTMS, 98 %), hexamethylsiloxane (HMDSO, 98 %), tetramethoxysilane (TMOS, 98 %) were obtained from Aladdin, China. BFs in form of fabric (420 g/m^2) were commercially available. Argon (Ar, 99.99 %) was supplied by Shenzhen Hongzhou Gas Industry Co., Ltd. All the materials were used as received.

2.2. Plasma deposition

The plasma deposition was carried out by a self-made atmospheric pressure plasma jet (APPJ) device powered by a 10 kHz high voltage power supply. Fig. 1 depicts the schematic of the plasma system, and the precursor was injected into the plasma together with the carrier gas. The working gas and carrier gas were both Ar, and the flow rates were constant at 3 SLM. Three different precursors (MTMS, HMDSO, and TMOS) were used for the deposition with a uniform flow rate of 20 ml/h, respectively. Fig. 2 shows the chemical structures of the three precursors. The BFs fabrics (50 mm × 50 mm) were placed below the plasma jet outlet, and the distance between the plasma outlet and the sample was set at 10 mm. Before deposition, the BFs fabrics were cleaned with Ar plasma for 180 s to remove surface impurities.

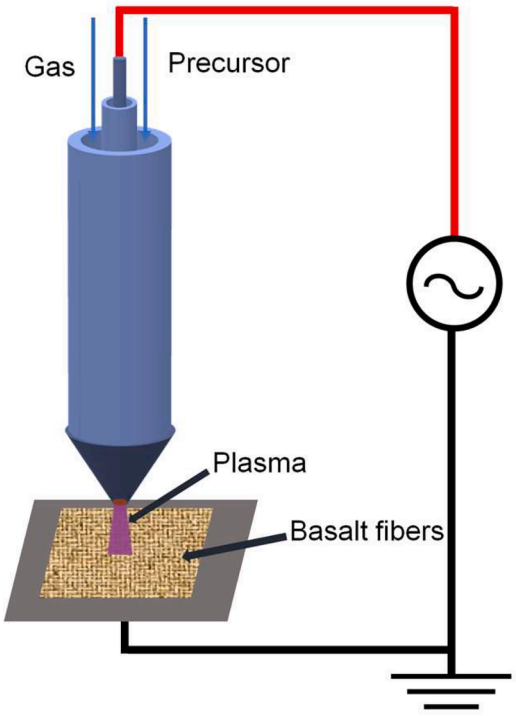

Fig. 1. Schematic of the plasma deposition apparatus.

2.3. Characterization

The surface morphology was observed by field-emission scanning electron microscopy (SEM, Supra 55, Zeiss, Germany). The surface chemical structure was analyzed by attenuated total reflection (ATR, Germanium crystals) Fourier transform infrared spectroscopy (FTIR, Nicolet iS50, Thermo Scientific, USA), and the FTIR spectra were performed from 600 to 4000 cm^{-1}. The surface chemical composition was determined by X-ray photoelectron spectroscopy (XPS, ESCALAB 250Xi, Thermo Fisher, USA), and all binding energies were referenced to the C *1 s* peak.

2.4. Thermal properties of the thin films

The thermal stability of the samples was determined with thermogravimetry (TG, 600, TA Instruments, USA). To evaluate the thermal insulation properties of the samples, a customized instrument was developed as shown in Fig. 3. The test apparatus was comprised of heat source, specimen fixed component, and measurement system, which was similar to the previous work [18]. The heat source with a temperature controller included hot plate and surface plate with a wide of 200 by 200 mm. A thermocouple was wrapped by six layered test specimen, and the wrapped thermocouple placed in an annular tube. One side of the tube was faced on the hot-plate, which was heated from room temperature to 250 °C. A temperature-time curve was obtained from the measurement system, and the measurement was repeated three times for each sample.

3. Results and discussion

3.1. Surface morphology

The surface morphology of the BFs observed by SEM is shown in Fig. 4. It is well known that the fabrics is woven from a large number of fiber strands, and the BFs strands are composed of several fibers with diameters of about 10 μm. The image in Fig. 4a depicts that the control sample has a relatively smooth surface. In comparison, the surfaces of the modified samples are different, and all the deposited sample (Fig. 4b–d) exhibit compact topography. Moreover, there are no evident defects such as pinholes or cracks that can be seen in the deposited sample. Fig. 5 shows the SEM images of the single fibers at high magnification, and the topography of the thin films on the BFs varies with the precursor types. As shown in Fig. 5a, the raw BFs possess a slippery and striped surface. In Fig. 5b, the BF-MTMS sample displays a thin layer structure with the individual nanoparticles. Using HMDSO as the precursor, the surface of the sample is well-defined with relatively clear (Fig. 5c). In the case of TMOS precursor, it can be seen from Fig. 5d that the sample exhibits a rough surface with tightly packed nanoparticles. The surface of the BF- TMOS sample is fully covered by the thin film composing of large nanoparticles. These nanoparticles are evenly distributed on the fiber surface, which may largely depend on the deposition process dominated by the formation of high molecular weight oligomers [19]. These various surface morphologies are highly dependent on the geometry of the initial molecular precursor [20].

3.2. Surface chemistry

Fig. 6 shows the FTIR spectra of the samples. Although the molecular structure of the studied precursor is different from each other, the FTIR spectra of the obtained films indicate a similar SiOx-based film structure for all of them. All the deposited thin films with different precursor show a shoulder absorption peak in the range of 900–1200 cm^{-1} represents the anti-asymmetric stretching of Si-O-C/Si-O-Si groups [21]. The peaks corresponding to Si-CH_3 groups at 1258 and 760–860 cm^{-1} can be observed [22]. The peaks in the region of 2750–3000 cm^{-1} corresponds to symmetric stretching vibrations of C–H bonds (2900 cm^{-1}) and

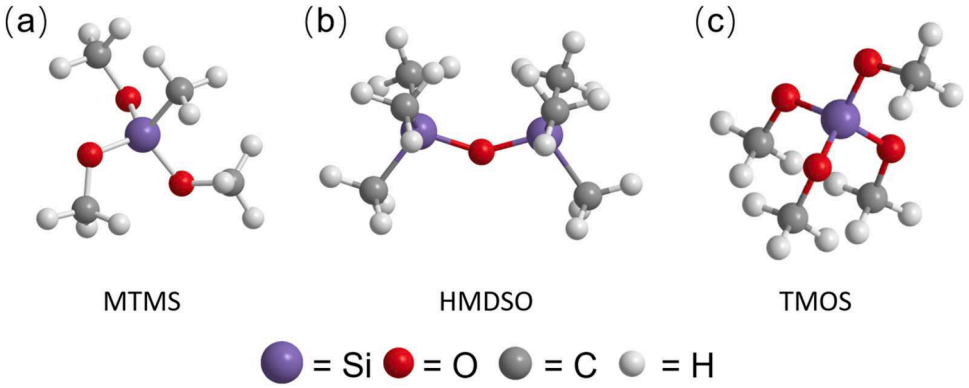

Fig. 2. Siloxane precursors used for the plasma deposition.

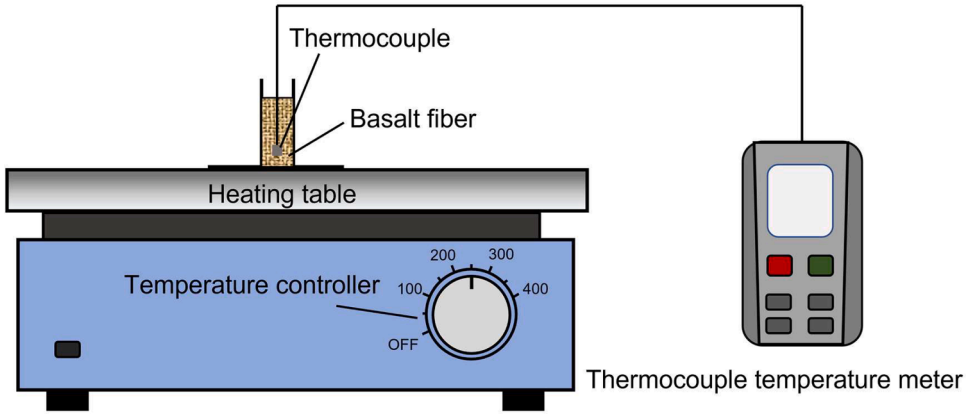

Fig. 3. Schematic diagram of the thermal insulation test system.

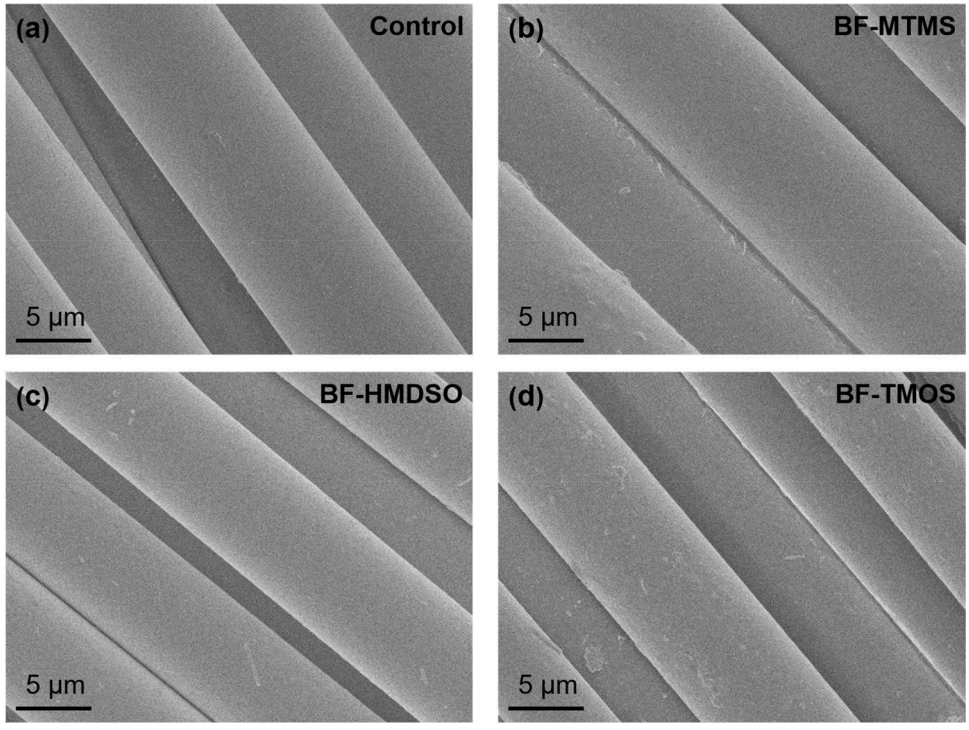

Fig. 4. SEM images of multiple fibers.

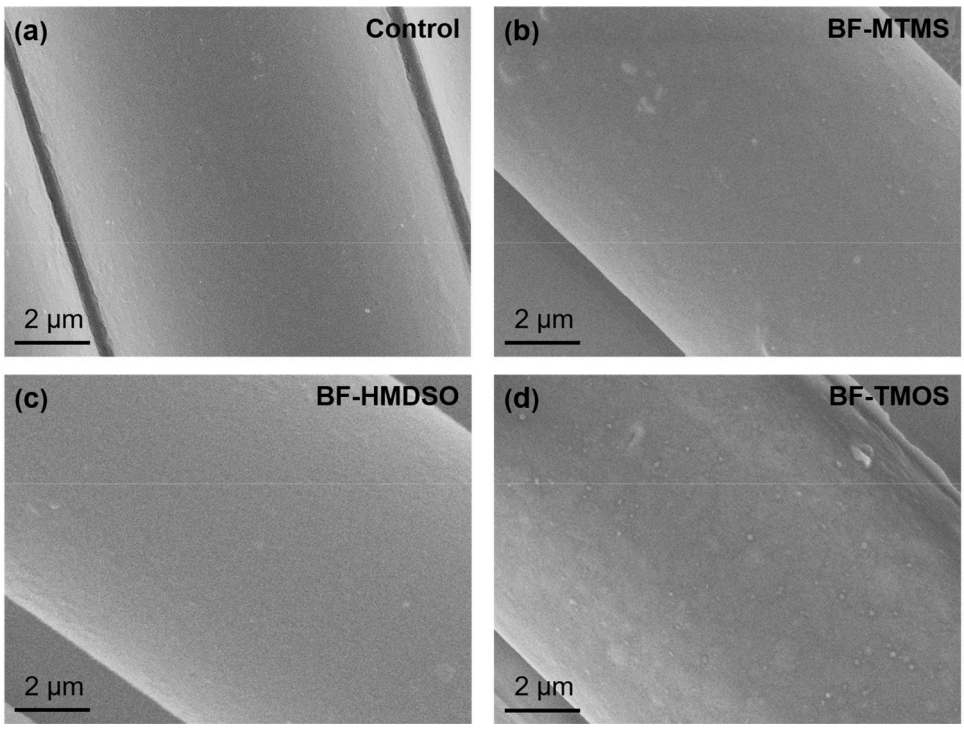

Fig. 5. SEM images of single fiber.

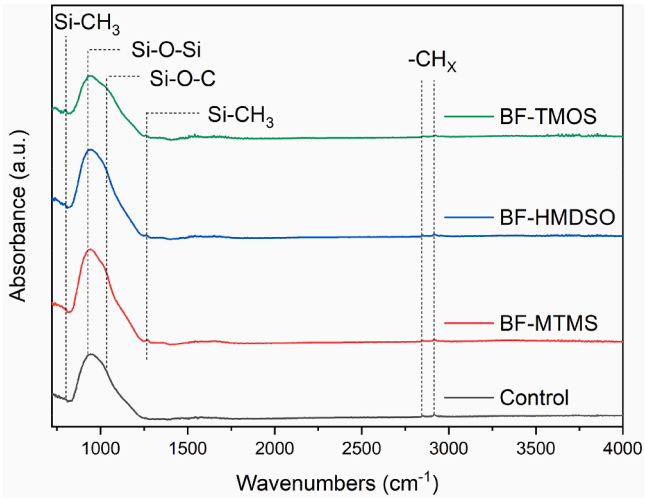

Fig. 6. FTIR spectra of the samples.

antisymmetric stretching vibrations of C–H bonds (2960 cm^{-1}) in methyl groups [23]. According to FTIR analysis, it can be concluded that the plasma deposition can modify the surface characteristics without any damage to its bulk properties.

XPS is used to further analyze the chemical composition of the samples. Table 1 shows the relative contents of C *1 s*, O *1 s*, and Si *2p*. The control sample surface consists of 5.61 % silicon, 14.92 % oxygen and 79.47 % carbon. For the samples with plasma modification, the concentration of carbon significantly decreases and the amount of silicon and oxygen increase. The average carbon content is about 44 % in all the plasma-deposited samples, which shows a 50 % reduction compared to the control sample. Regarding the change in the ratios of O/C and Si/C, a considerable increase of relative oxygen and silicon concentration can be seen. These results demonstrate that plasma deposition can lead to the thin films with much less carbon and more oxygen and silicon than that of the control samples.

Table 1
Elemental composition of the thin films under different precursors.

Relative atomic ratio (%)	C1s	O1s	Si2p	O/C	Si/C
Control	77.8	14.61	5.49	0.18	0.07
BF-MTMS	40.15	38.83	19.26	0.97	0.47
BF-HMDSO	47.52	33.21	17.26	0.70	0.36
BF-TMOS	44.13	36.09	16.43	0.82	0.37

To further reveal the impact of the precursor on the surface chemical composition of the prepared thin films, the high-resolution XPS Si*2p* spectra were collected and shown in Fig. 7. On the surface of the control sample (Fig. 7a), it could be easily found that a characteristic peak of Si-O-Si structure is at 102.2 eV and the peak belonging to C-Si-O is at 101.7 eV [24]. After the plasma deposition, all the spectra acquired at different precursors can also show the formation of Si-O-Si structure at 102.2 eV. However, different chemical components are presented in the different spectra. Similar with the control sample, the spectra of the BF-MTMS samples (Fig. 7b) can be decomposed into two components. Apart from the Si-O-Si structure, the Si-O component is shown at 103.0 eV, which is associated to Si-O bonds (Si_xO_y) [25]. For the BF-HMDSO and BF-TMOS samples, the spectra can be deconvoluted into three peaks, including two components at 102.2 eV and 103.0 eV. Additionally, the peak corresponding to C-Si-O (101.7 eV) can be seen in the spectrum of the BF-HMDSO samples (Fig. 7c). Specifically, the spectrum of the BF-TMOS sample (Fig. 7d) presents the SiO_x at 103.5 eV [26]. These results suggest that the bonding environment of the silicon depends on the starting siloxane precursors.

3.3. *Thermal stability of the thin films*

The thermogravimetric analysis is used to evaluate the thermal stability behavior of the thin films, and the TG curves obtained in the air atmosphere by temperature scanning from room temperature to 600 °C at a heating rate of 20 °C/min are shown in Fig. 8. Generally, when heat transfers to the surface of materials uniformly, the fraction of heat has been absorbed by the coating or thin film on the surface [27]. Moreover,

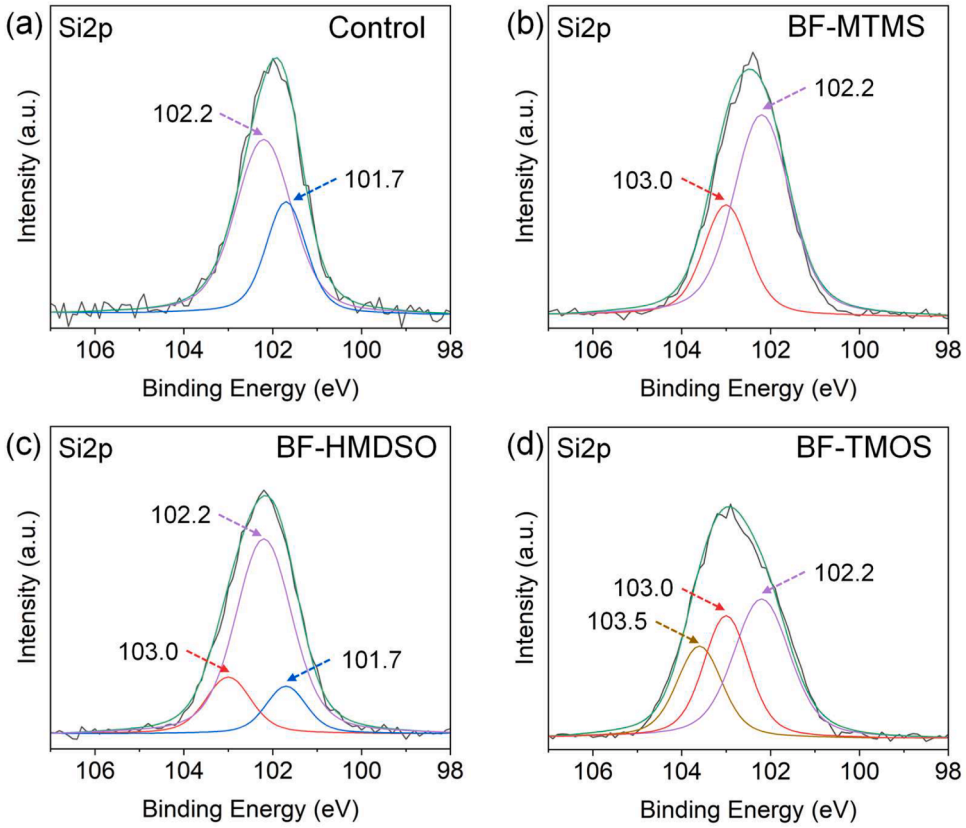

Fig. 7. Si XPS spectra of the samples.

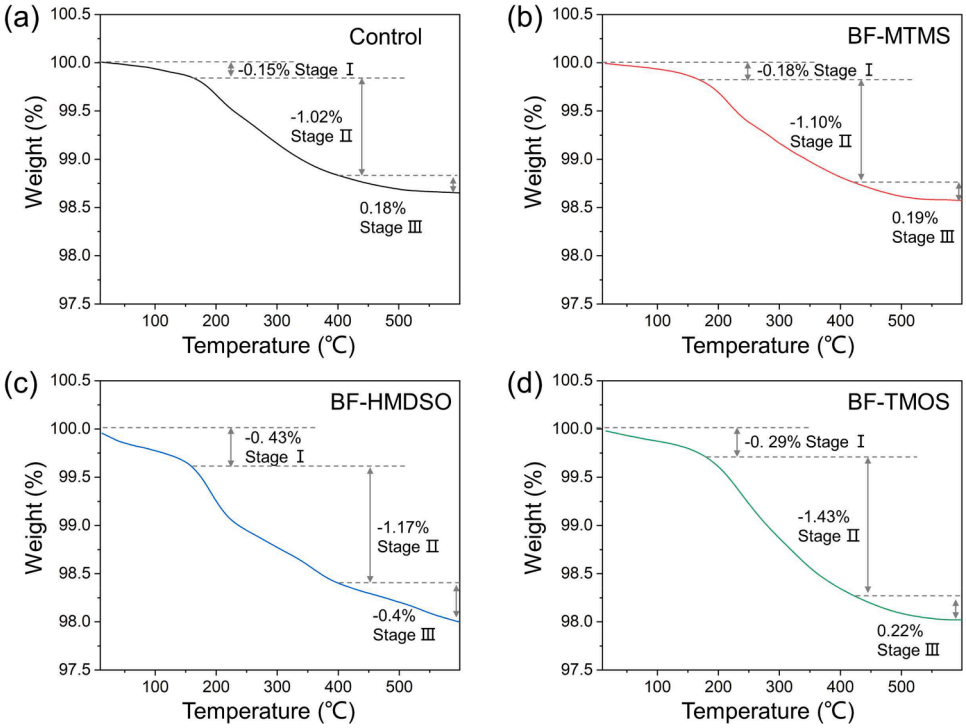

Fig. 8. TG curves of the samples.

as thermally stable materials, BFs can present a residual weight of 99 % after 900 °C [28]. Therefore, the sharp of the TG curves depends on the coating or thin film on the fiber surface. For all the deposited samples, a negligible mass loss (Stage I) can be seen in the three samples below 200 °C, which may attribute to the residual water molecules. After temperature rises above 200 °C, the main weight loss (stage II) occurs in all the

deposited samples, which may due to the condensation of Si-OH and the gasification of the molecular fragmentation [29,30]. When the temperature exceeds 450 °C, a further weight loss can be seen in all deposited samples (Stage III), which may be ascribed to the breakage of the segments on the organosilicon chain [31,32]. Taking into account the weight loss, all the deposited samples present a weight loss less than 2 %, indicating that the thermal stability of the thin films by plasma deposition is appropriate.

3.4. Thermal insulation performance of the thin films

Since basalt fiber is mainly applied as an efficient thermal insulation material, the thermal insulation performance of the thin films on the fiber was tested. When the tested fabrics with different thin films are contacted to the heating plate, the thermal energy from the hot plate is transmitted to the fabric. The thermal insulation performance can be determined from inner surface temperature of the fabric, which can be obtained by the thermocouple. Fig. 9 depicts the average value of temperature changes and the resulted temperature change curve. It is clear that the inner surface temperatures of all the fabrics increase rapidly during the heat exposure, and the contact surface temperature for all the fabrics show the same changing tendency over the time. From ambient, the temperature rises to 180 °C in less than 90 s. At this point, there was no significant difference between the deposited samples and the control sample. However, an obvious changing tendency for the surface temperature of the different deposited fabrics is observed after heating for 90 s. Compared with the control sample, the presence of the thin film on the fiber reduces the heat transfer through fabrics via convection and conduction hence a lower surface temperature can be observed. This can prove the role of the thin film in preventing rapid heat conduction from the hot plate to the deposited fabrics. In the deposited samples, the surface temperatures of the BF-HMDSO sample and the BF- TMOS sample are lower than that of the BF-MTMS sample. The reason may be that the difference in the spatial structure of the thin films prepared by different precursors can result in a variation in thermal resistance [33–35]. The structure will prevent the rate of heat conduction inside the thin films, allowing less energy transferred, thereby lowering the surface temperature of the fabrics.

It is well known that the concept of introducing surface coatings in the fabric structures has already been used to improve the thermal insulation performance [36]. The coatings or thin films can introduce a layer on fabrics with low thermal conductivity, which are essential in thermal insulation [37]. Generally, the thermal insulation performance is sensitive to measuring apparatuses, sample size, sample moisture content, ambient temperature and humidity and so on, when the BFs materials are placed in the real environment [38]. A number of factors such as heat flux and mode, part geometry and location, thin films type and its thermal conductivity, determine the magnitude of temperature reduction of the substrate [39]. In this work, the coatings on BFs surface by atmospheric pressure plasma deposition are very thin, resulting in a limited temperature reduction. However, on account of the excellent activity and great thermal resistance of Si–O–Si networks, the BFs surface can be successfully modified. Moreover, it is significant to develop thin films on the BFs surface that can modify the surface with improved thermal insulation for practical application. Based on the findings of this research, it was demonstrated that the thin films prepared by atmospheric pressure plasma deposition can present improved features of thermal insulation, which offers a promising alternative to conventional plasma treatment techniques for surface modification.

4. Conclusion

In summary, a simple atmospheric pressure plasma deposition approach for surface modification of BFs has been proposed. Three different siloxane precursors are applied to form thin film on the BFs surface, and the precursors can affect the surface morphology, surface chemical structure, and the thermal mass loss of the thin film. Following the thermal insulation test, the surface temperature of the BF-TMOS sample is lower than that of the BF-MTMS sample and BF-HMDSO sample, because of its relatively high surface roughness and more Si-O-Si network. These results suggest that the thin film prepared by plasma deposition could enhance the advanced properties of the BFs. In conclusion, the use of atmospheric pressure plasma deposition in combination with an appropriate precursor is an effective strategy to surface modification of flexible materials with improved properties.

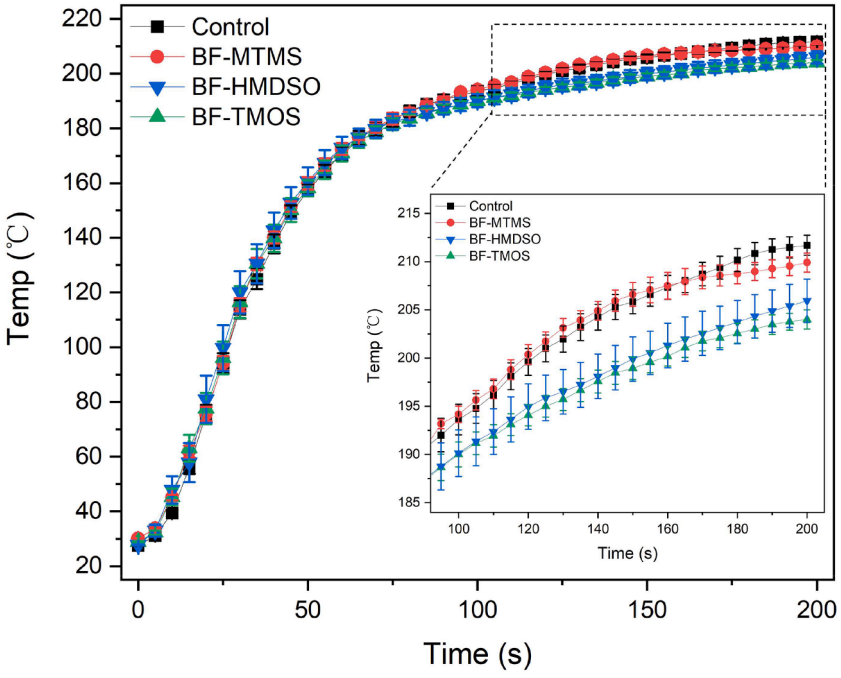

Fig. 9. Time dependence of surface temperature of the samples.

CRediT authorship contribution statement

Chengfeng Xiong: Conceptualization, Investigation, Writing – original draft. **Ming Gao:** Conceptualization, Supervision, Writing – review & editing. **Hao Huang:** Formal analysis, Methodology. **Yu Wang:** Data curation, Investigation. **Xiaobin Gu:** Methodology, Resources. **Zilan Xiong:** Funding acquisition, Resources. **Yifan Huang:** Supervision, Validation.

Declaration of competing interest

The authors declare that they have no known competing financial interests or personal relationships that could have appeared to influence the work reported in this paper.

Data availability

Data will be made available on request.

Acknowledgments

This work was funded by Shenzhen Science and Technology Innovation Committee (No. JSGG20210802153408024 and JCYJ20190806165216555) and Interdisciplinary Fund of the Wuhan National High Magnetic Field Center (No. WHMFC202101).

References

[1] S. Khandelwal, K.Y. Rhee, Recent advances in basalt-fiber-reinforced composites: tailoring the fiber-matrix interface, Compos. B Eng. 192 (2020) 108011, https://doi.org/10.1016/j.compositesb.2020.108011.
[2] Y. Li, J. Zhang, Y. He, G. Huang, J. Li, Z. Niu, B. Gao, A review on durability of basalt fiber reinforced concrete, Compos. Sci. Technol. 225 (2022) 109519, https://doi.org/10.1016/j.compscitech.2022.109519.
[3] S.H. Kim, J.H. Lee, J.W. Kim, S.Y. Lee, S.J. Park, Interfacial behaviors of basalt fiber-reinforced polymeric composites: a short review, Adv. Fiber Mater. 4 (2022) 1414–1433, https://doi.org/10.1007/s42765-022-00204-0.
[4] P.T. Benyei, P. Santha, Potential applications of basalt fibre composites in thermal shielding, J. Therm. Anal. Calorim. 148 (2023) 271–279, https://doi.org/10.1007/s10973-022-11799-2.
[5] K.V. Balaji, K. Shirvanimoghaddam, G.S. Rajan, A.V. Ellis, M. Naebe, Surface treatment of basalt fiber for use in automotive composites, Mater. Today Chem. 17 (2020) 100334, https://doi.org/10.1016/j.mtchem.2020.100334.
[6] P. Sundriyal, M. Pandey, S. Bhattacharya, Plasma-assisted surface alteration of industrial polymers for improved adhesive bonding, Int. J. Adhes. Adhes. 101 (2020) 102626, https://doi.org/10.1016/j.ijadhadh.2020.102626.
[7] E.O. Ortega, S. Hosseini, S.O.M. Chapa, M.J. Madou, Aging of plasma-activated carbon surfaces: challenges and opportunities, Appl. Surf. Sci. 565 (2021) 150362, https://doi.org/10.1016/j.apsusc.2021.150362.
[8] A. Michelmore, J.D. Whittle, J.W. Bradley, R.D. Short, Where physics meets chemistry: thin film deposition from reactive plasmas, Front. Chem. Sci. Eng. 10 (2016) 441–458, https://doi.org/10.1007/s11705-016-1598-7.
[9] S. Yu, K.H. Oh, S.H. Hong, Enhancement of the mechanical properties of basalt fiber-reinforced polyamide 6,6 composites by improving interfacial bonding strength through plasma-polymerization, Compos. Sci. Technol. 182 (2019) 107756, https://doi.org/10.1016/j.compscitech.2019.107756.
[10] M. Lilli, M. Zvonek, V. Cech, C. Scheffler, J. Tirillo, F. Sarasini, Low temperature plasma polymerization: an effective process to enhance the basalt fibre/matrix interfacial adhesion, Compos. Commun. 27 (2021) 100769, https://doi.org/10.1016/j.coco.2021.100769.
[11] Y. Xu, T. He, Y. Zhang. H. Wang, Y. Guo, J. Shi, C. Du, J. Zhang, Insights into the low-temperature deposition of a dense anatase TiO_2 film via an atmospheric pressure pulse-modulated plasma, Plasma Process Polym. 18 (2021) 2100050, https://doi.org/10.1002/ppap.202100050.
[12] E. Eslami, R. Jafari, G. Momen, A review of plasma-based superhydrophobic textiles: theoretical definitions, fabrication, and recent developments, J. Coat. Technol. Res. 18 (2021) 1635–1658, https://doi.org/10.1007/s11998-021-00523-8.
[13] A.S. Bil, S.E. Alexandrov, The effect of the process parameters on the growth rate and composition of the anti scratch films deposited from TEOS by AP-PECVD on polycarbonate, Plasma Chem. Plasma Process. 43 (2023) 901–902, https://doi.org/10.1007/s11090-023-10331-0.
[14] M.A. Gilliam, S.A. Farhat, G.E. Garner, B.P. Stubbs, B.B. Peterson, Characterization of the deposition behavior and changes in bonding structures of hexamethyldisiloxane and decamethylcyclopentasiloxane atmospheric plasma-deposited films, Plasma Process. Polym 16 (2019) e1900024, https://doi.org/10.1002/ppap.201900024.
[15] M. Gao, Y. Wang, Y. Zhang, Y. Li, Y. Tang, Y. Huang, Deposition of thin films on glass fiber fabrics by atmospheric pressure plasma jet, Surf. Coat. Technol. 404 (2020), https://doi.org/10.1016/j.surfcoat.2020.126498.
[16] I.R. Duran, J. Profili, L. Stafford, G. Laroche, Unveiling the origin of the anti-fogging performance of plasma-coated glass: role of the structure and the chemistry of siloxane precursors, Prog. Org. Coat. 141 (2020) 105401, https://doi.org/10.1016/j.porgcoat.2019.105401.
[17] T. Egghe, M. Narimisa, R. Ghoberia, B. Nisol, Y. Onyshchenko, R. Hoogenboom, R. Morent, N.D. Geyter, Comparison of the physicochemical properties and aging behavior of two different APTES-derived plasma polymer-based coatings, Surf. Coat. Technol. 449 (2022) 128945, https://doi.org/10.1016/j.surfcoat.2022.128945.
[18] Y. Su, J. Yang, R. Li, G. Song, J. Li, Experimental study of moisture role and heat transfer in thermal insulation fabric against hot surface contact, Int. J. Therm. Sci. 156 (2020) 106501, https://doi.org/10.1016/j.ijthermalsci.2020.106501.
[19] F. Fanelli, S. Lovascio, R. Agostino, F. Fracassi, Insight into the atmospheric pressure plasma-enhanced chemical vapor deposition of thin films from methyldisiloxane precursors, Plasma Process. Polym. 9 (2012) 1132, https://doi.org/10.1002/ppap.201100157.
[20] R.K. Gangwar, A. Hamdan, L. Stafford, Nanoparticle synthesis by high-density plasma sustained in liquid organosilicon precursors, J. Appl. Phys. 122 (2017) 243301, https://doi.org/10.1063/1.5006479.
[21] R. Wang, C. Cui, C. Zhang, C. Ren, G. Chen, T. Shao, Deposition of SiOx film on electrode surface by DBD to improve the lift-off voltage of metal particles, IEEE Trans. Dielectr. Electr. Insul. 25 (2018) 1285–1292, https://doi.org/10.1109/TDEI.2018.007157.
[22] M. Kawasaki, H. Nagasawa, M. Kanezashi, T. Tsuru, Open-air plasma deposition of polymer-supported silica-based membranes for gas separation, Sep. Purif. Technol. 291 (2022) 120908, https://doi.org/10.1016/j.seppur.2022.120908.
[23] D.A. Zuza, V.O. Nekhoroshev, A.V. Batrakov, A.B. Markov, I.A. Kurzina, Characterization of hexamethyldisiloxane plasma polymerization in a DC glow discharge in an argon flow, Vacuum 207 (2023) 111690, https://doi.org/10.1016/j.vacuum.2022.111690.
[24] Y. Guo, H. Lu, X. Jian, SiO_2–modified APTMS nanocoatings encapsulating FeNi: amplifying microwave absorption and corrosion resistance, Appl. Surf. Sci. 652 (2024) 159286, https://doi.org/10.1016/j.apsusc.2023.159286.
[25] M. Pereira, E.K. Baldin, L.M. Antonini, F. Bernardi, L. Oliveira, N. Maurmann, P. Pranke, M.B. Pereira, C.D.F. Malfatti, TEOS thin films obtained by plasma polymerization on Ti_6Al_4V alloys: influence of the deposition pressure on surface properties and cellular response, Appl. Surf. Sci. Adv. 5 (2021) 100123, https://doi.org/10.1016/j.apsadv.2021.100123.
[26] X. Xie, D. Zanders, F. Preischel, T.D.L. Arcos, A. Devi, G. Grundmeier, Complementary spectroscopic and electrochemical analysis of the sealing of micropores in hexamethyldisilazane plasma polymer films by Al_2O_3 atomic layer deposition, Surf. Interf. Anal. 55 (2023) 886–898, https://doi.org/10.1002/sia.7256.
[27] Z.Y. Zhang, L. Yuan, G.Z. Liang, A.J. Gu, A strategy and mechanism of fabricating flame retarding glass fiber fabric reinforced vinyl ester composites with simultaneously improved thermal stability, impact and interlaminar shear strengths, Polym. Degrad. Stabil. 125 (2016) 49–58, https://doi.org/10.1016/j.polymdegradstab.2016.01.002.
[28] M. Yasir, F. Ahmad, P.S.M. Megat-Yusoff, S. Ullah, M. Jimenez, Quantifying the effects of basalt fibers on thermal degradation and fire performance of epoxy-based intumescent coating for fire protection of steel substrate, Prog. Org. Coat. 132 (2019) 148–158, https://doi.org/10.1016/j.porgcoat.2019.03.019.
[29] F. Sohbatzadeh, A. Shabannejad, M. Ghasemi, Z. Mahmoudsani, Deposition of halogen-free flame retardant and water-repellent coatings on firwood surfaces using the new version of DBD, Prog. Org. Coat. 151 (2021) 106070, https://doi.org/10.1016/j.porgcoat.2020.106070.
[30] C. Yao, X. Dong, G. Gao, F. Sha, D. Xu, Microstructure and adsorption properties of MTMS /TEOS co-precursor silica aerogels dried at ambient pressure, J. Non Cryst. Solids 562 (2021) 120778, https://doi.org/10.1016/j.jnoncrysol.2021.120778.
[31] J. Mo, W. Ma, G. Qiu, Y. Shi, Mesoporous silica coated graphene oxide: fabrication, characterization and effects on the dielectric properties of its organosilicon hybrid films, J. Mater. Sci. Mater. Electron. 30 (2019) 130–146, https://doi.org/10.1007/s10854-018-0275-7.
[32] V. Purcar, V. Raditoiu, A. Raditoiu, F.M. Raduly, G.C. Lspas, S. Caprarescu, A. N. Frone, B. Trica, C.A. Nicolae, M. Anastasescu, H. Stroescu, Effect of modified silica materials on polyvinyl chloride (PVC) substrates to obtain transparent and hydrophobic hybrid coatings, Appl. Sci. 11 (2021) 11044, https://doi.org/10.3390/app112211044.
[33] R.B. Torres, J.P. Vareda, A.L. Mendes, L. Duraes, Effect of different silylation agents on the properties of ambient pressure dried and supercritically dried vinyl-modified silica aerogels, J. Supercrit. Fluids 147 (2019) 81–89, https://doi.org/10.1016/j.supflu.2019.02.010.
[34] S. Karamikamkar, H.E. Naguib, C.B. Park, Advances in precursor system for silica-based aerogel production toward improved mechanical properties, customized morphology, and multifunctionality: a review, Adv. Colloid Interf. Sci. 276 (2020) 102101, https://doi.org/10.1016/j.cis.2020.102101.
[35] X. Mei, S. Li, Y. Chen, X. Huang, Y. Cao, V.P. Guro, Y. Li, Silica-chitosan composite aerogels for thermal insulation and adsorption, Crystals 13 (2023) 755, https://doi.org/10.3390/cryst13050755.
[36] A.L. Davesne, M. Jimenez, F. Samyn, S. Bourbigot, Thin coatings for fire protection: an overview of the existing strategies, with an emphasis on layer-by-layer surface

treatments and promising new solutions, Prog. Organ. Coat. 154 (2021) 106217, https://doi.org/10.1016/j.porgcoat.2021.106217.
[37] J. Wu, M. Zhang, M. Su, Y. Zhang, J. Liang, S. Zeng, B. Chen, L. Cui, C. Hou, G. Tao, Robust and flexible multimaterial aerogel fabric toward outdoor passive heating, Adv. Fiber Mater. 4 (2022) 1545, https://doi.org/10.1007/s42765-022-00188-x.
[38] W. Yang, Y. Wang, J. Liu, Optimization of the thermal conductivity test for building insulation materials under multifactor impact, Constr. Build Mater. 332 (2022) 127380, https://doi.org/10.1016/j.conbuildmat.2022.127380.
[39] V. Kumar, K. Balasubramanian, Progress update on failure mechanisms of advanced thermal barrier coatings: a review, Prog. Org. Coat. 90 (2016) 54–82, https://doi.org/10.1016/j.porgcoat.2015.09.019.